*Original Research* *Highlight article*

# Dissecting the ferroptosis-related prognostic biomarker and immune microenvironment of driver gene-negative lung cancer

**Rui Zhou[1], Hao-chuan Ma[1], Yi-hong Liu[2], Xian Chen[1,2], Xue-song Chang[2], Ya-dong Chen[2], Li-rong Liu[2], Yong Li[2], Yan-juan Zhu[1,2,3,4] and Hai-bo Zhang[2,3,4,5]**

[1]The Second Clinical Medical School of Guangzhou University of Chinese Medicine, Guangzhou 510405, China; [2]Department of Oncology, The Second Affiliated Hospital of Guangzhou University of Chinese Medicine, Guangdong Provincial Hospital of Traditional Chinese Medicine, Guangzhou 510120, China; [3]Guangdong-Hong Kong-Macau Joint Lab on Chinese Medicine and Immune Disease Research, Guangzhou 510120, China; [4]Guangdong Provincial Key Laboratory of Clinical Research on Traditional Chinese Medicine Syndrome, Guangzhou 510120, China; [5]State Key Laboratory of Dampness Syndrome of Chinese Medicine, The Second Affiliated Hospital of Guangzhou University of Chinese Medicine, Guangzhou 510120, China
Corresponding authors: Hai-bo Zhang. Email: haibozh@gzucm.edu.cn; Yan-juan Zhu. Email: zyjsophy@gzucm.edu.cn

### Impact Statement

Despite substantial advances in targeted and immune therapy for NSCLC, viable treatments for driver-negative NSCLC with low PD-L1 expression remain unresolved. While some of these patients might benefit from immune checkpoint inhibitors (ICIs), a more precise predictor is also needed to identify highly susceptible individuals. Ferroptosis is essential for antitumor action. Our findings indicated a link between ferroptosis and both OS and the immune microenvironment. Moreover, we constructed an eight-gene signature (risk score = [−0.024**CLIC6*] + [−0.044**ADH1C*] + [0.023**CPS1*] + [0.018**STC2*] + [0.007**ABCC2*] + [0.041**KLK8*] + [0.067**INSL4*] + [−0.005**CHST9*]), which negatively correlated with patient prognosis and immunotherapy response. Collectively, our findings may contribute to a better understanding of the biological role of ferroptosis in *EGFR*/*ALK*$^{WT}$ NSCLC with low-level PD-L1, providing a robust basis for developing new therapeutic strategies.

### Abstract

Despite significant advances in targeted and immune therapy for non-small cell lung cancer (NSCLC), effective therapies for wild-type epidermal growth factor receptor/anaplastic lymphoma kinase (*EGFR*/*ALK*$^{WT}$) with low expression of programmed death ligand-1 (PD-L1) NSCLC remain elusive. Numerous studies have shown that ferroptosis plays an essential role in antitumor activity. To identify the molecular regulation patterns associated with ferroptosis, 351 *EGFR*/*ALK*$^{WT}$ NSCLC samples with low-level PD-L1 were extracted from The Cancer Genome Atlas (TCGA) and clustered using the k-means clustering technique. The two clusters associated with ferroptosis showed significantly different prognoses. In total, 169 differential expression genes (DEGs) were identified. Cluster differential analysis revealed that Cluster 1 had a significantly poorer overall survival (OS) and was associated with more negative immune regulation. In addition, TCGA samples were randomly assigned in a 7:3 ratio to a training group or testing group. A signature of eight genes associated with ferroptosis was established in the training cohort using DEGs and validated in the test cohort and three independent cohorts (GSE72049, GSE41271, and GSE50081). The 5-year area under the curve (AUC) was 0.713, which was significantly higher than that of other predictors, including TNM stage and age. Furthermore, the risk score was associated with immune function, immune infiltration, and immunotherapy response, with high-risk patients having a worse prognosis, an immune-suppressing phenotype, and a poor response to immune checkpoint inhibitors. This study aims to contribute to our understanding of the biological role of ferroptosis in *EGFR*/*ALK*$^{WT}$ NSCLC with low-level PD-L1, laying the groundwork for the development of novel therapeutic strategies.

**Keywords:** Ferroptosis, *EGFR*/*ALK*$^{WT}$, low PD-L1 expression, NSCLC, prognosis, immune microenvironment

***Experimental Biology and Medicine* 2022; 247: 1447–1465. DOI: 10.1177/15353702221102872**

## Introduction

Lung cancer has long been the leading cause of cancer-related mortality worldwide,[1] with NSCLC accounting for more than 80% of lung cancer diagnoses. The advent of small-molecule drugs targeting specific signaling pathways has resulted in a significant breakthrough by markedly extending progression-free survival (PFS) and overall survival (OS) for NSCLC patients with epidermal growth factor receptor (*EGFR*)-sensitive mutation or anaplastic lymphoma kinase (*ALK*) fusion/mutation.[2,3] Furthermore, immune checkpoint inhibitors (ICIs) targeting programmed death receptor-1

(PD-1) and its ligand (PD-L1) have considerably extended the OS of wild-type epidermal growth factor receptor/anaplastic lymphoma kinase (*EGFR/ALK*$^{WT}$) non-small cell lung cancer (NSCLC) patients with positive PD-L1 (>1%).[4,5] However, effective treatment modalities remain elusive for *EGFR/ALK*$^{WT}$ and negative PD-L1 expression (<1%) NSCLC patients, which accounts for about 40% of lung cancers.[6,7] While multidrug combinations have clinically been used as a last resort for this population, this has also led to a significantly increased number of reported adverse events.[5,8,9] Although a handful of NSCLCs with negative PD-L1 could respond to ICIs,[6,7] it is difficult to identify this subset of people due to the lack of an accurate biomarker. As a result, additional efforts are needed to develop novel therapeutic strategies for NSCLC with *EGFR/ALK*$^{WT}$ and negative PD-L1 expression.

Ferroptosis is a particular programmed cell death involving the iron-dependent accumulation of lipid hydroperoxides to lethal levels.[10,11] Mounting studies have indicated that ferroptosis is associated with various antitumor activities.[12] For instance, the ferroptosis activators RSL3 and erastin were selectively lethal against tumors with *RAS* mutation, and the activation of ferroptosis cell death could reverse the resistance of cancer cells to chemotherapy.[13,14] Furthermore, ferroptosis has a synergistic effect with anti-PD-L1 antibodies, which can be boosted or diminished by ferroptosis activators or inhibitors, respectively.[15] Nevertheless, damage-associated molecular patterns released during ferroptotic cell death also have a tumor-promoting effect. HMGB1 has been shown to induce inflammatory responses that promote tumor growth,[16] and *KRAS-G12D* can polarize macrophages to an M2 phenotype, resulting in immunosuppression.[17] The interaction between ferroptosis and antitumor activity is still poorly understood, and additional research is required.

Herein, the effect of 24 ferroptosis-related genes on prognosis and the immune microenvironment in *EGFR/ALK*$^{WT}$ low PD-L1 expression NSCLC patients was evaluated. The 351 samples were clustered according to the levels of ferroptosis regulators, and two subtypes, which were significantly different in OS and immune function, were identified. Based on the differential expression genes (DEGs) between the clusters, a scoring model was generated by univariate and least absolute shrinkage and selection operator (LASSO) penalty Cox regression. Importantly, our signature model could predict OS, tumor immune microenvironment (TIME), and the response to ICIs. Our current findings suggested a potential association between ferroptosis, prognosis, TIME, and immunotherapy responsiveness in *EGFR/ALK*$^{WT}$ NSCLC patients with low-level PD-L1.

## Materials and methods

The study flow chart is shown in Figure 1.

### Datasets and preprocessing

The current study included lung adenocarcinoma and squamous cell carcinoma patients from The Cancer Genome Atlas (TCGA) database (accessed December 2021). Genome, transcriptome, and clinical data were downloaded on 16 December 2021. According to previous studies,[6,7] about 40% of NSCLC showed negative PD-L1 expression; therefore, PD-L1 transcript levels lower than 40% were defined as low expression. After excluding *EGFR/ALK*-mutant and high PD-L1 expression samples, 351 tumor and 107 paracancer tissue samples were selected. The expression data were normalized to transcripts per million (TPM), and batch effects were removed using the "RemoveBatchEffect" function in the limma package (version 3.46.0).[18] We downloaded three NSCLC datasets (GSE72049, GSE41271, and GSE50081) from Gene Expression Omnibus (GEO, accessed December 2021) as independent validation sets. All the analyses were implemented using R software (version 4.0.3, accessed December 2021–January 2022).

### Genetic mutation, expression, and interaction of ferroptosis-related genes

Overall, 24 ferroptosis-related genes (Supplementary Table S1) were identified by previous studies.[11] The genetic landscape of *EGFR/ALK*$^{WT}$ low-level PD-L1 NSCLC was generated using the Maftools package (version 2.6.05).[19] The expression of 24 regulators in tumors and paracancer tissues was compared using the Wilcox test. A protein–protein interaction (PPI) network for ferroptosis-related genes was generated using the Search Tool for the Retrieval of Interaction Genes (STRING version 11.0, accessed December 2021). R packages ggplot2 (version 3.3.5), reshape (version 0.8.8), and igraph (version 1.2.7) were also utilized in these procedures.[20]

### Unsupervised clustering

The k-means clustering method was adopted to classify 351 samples into different subtypes based on the transcript levels of 24 ferroptosis-related genes. The process was repeated 1000 times to achieve a robust classification,[21] and the number of clusters was adjusted using the consensus algorithm.[22]

### Identification of DEGs and function annotation

To identify DEGs between two ferroptosis-related clusters, the limma package was used with the significance criteria of $|\log_2\text{-fold change}| > 0.8$ and false discovery rate (FDR) $< 0.05$. Gene enrichment analysis was conducted using MetaScape (www.metascape.org, version 3.5.20220101, accessed December 2021). To identify the molecular characteristic, gene set enrichment analysis (GSEA) was conducted based on "c2.cp.kegg.v7.4.symbols" and "c5.go.bp.v7.4.symbols" from the MSigDB database (accessed December 2021).

### Construction of a ferroptosis-related prognostic signature

All *EGFR/ALK*$^{WT}$ and low PD-L1 NSCLC samples were randomly assigned to a training or testing group in a 7:3 ratio. We first screened prognosis-related DEGs using univariate Cox regression in the training group with a cutoff value of 0.05. LASSO regression was then implemented to select the candidate markers and generate a ferroptosis-related prognostic signature (glmnet package, version 4.1-2).[23] Patients

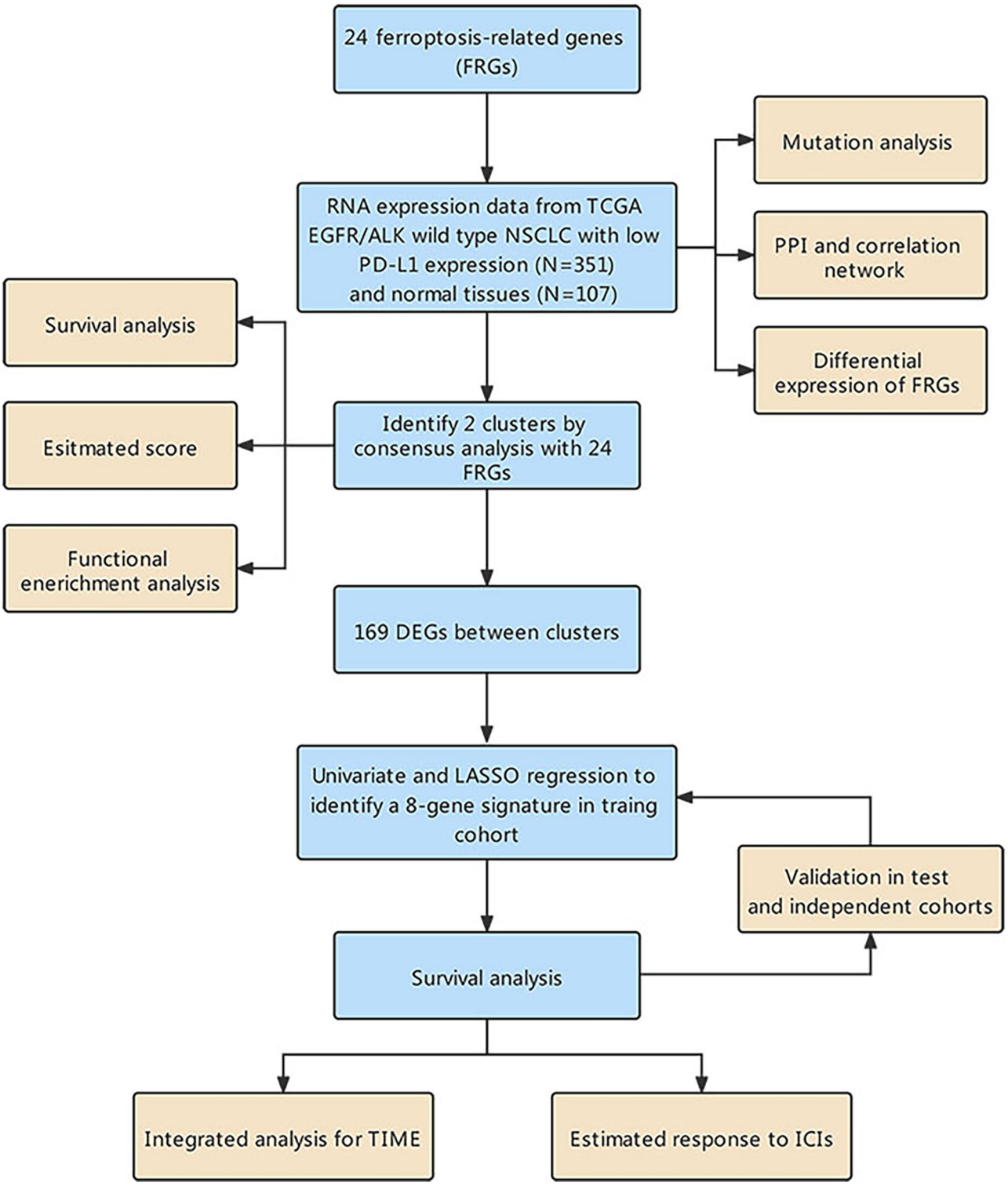


**Figure 1.** Workflow diagram. The flow chart of data analysis. (A color version of this figure is available in the online journal.)

were classified as high or low risk according to the median value of risk scores in the training set. Survival analysis between the two risk groups was carried out using the Kaplan–Meier method (survival and survivalROC package, version 3.2-13 and 1.0.3, respectively).[24] The predictive power of the ferroptosis-related model was evaluated using the time-dependent receiver operating characteristic (ROC) curve. The ferroptosis-related model was further validated in the testing group and three independent cohorts.

### Estimation of immune microenvironment feature

The immune score of all samples was calculated using the R package ESTIMATE (version 1.0.13).[25] The ESTIMATE

algorithm consists of an "immune score" parameter and two non-immune parameters, "stromal score" and "tumor purity." We also revealed the immunologic characteristics between groups using multiple acknowledged algorithms, such as XCELL, MCPcounter, and CIBERSORT. Correlation coefficients between the risk score and diverse immune-infiltrating cells were obtained using the spearman correlation method. The estimation data were downloaded from TIMER 2.0 (http://timer.cistrome.org/, accessed January 2022). The R packages tidyverse (version 1.3.1) and ggplot2 (version 3.3.5) were also utilized.

Based on published studies, 29 immune-related gene sets were selected,[26] representing distinct immune cells and functions. Each sample's immune biological role and physiological function scores were quantified through single-sample GSEA (ssGSEA).

### Estimation of immunotherapy response

According to the expression of immune biomarkers, a solid tumor can be roughly divided into two categories, immunologically hot or cold tumors, of which hot tumors are more sensitive to immunotherapy.[27] The association between the risk score and immunological cluster was assessed by dividing all samples into hot or cold tumors using an unsupervised clustering method. In addition, the immunophenoscore (IPS) for each sample was calculated using The Cancer Immunome Database (TCIA, accessed January 2022). TCIA provides an IPS based on tumor immunogenicity identified by a random forest approach, and a higher IPS often, but not always, suggests a better response to ICIs.[28,29]

### Statistical analysis

The normality of continuous data was evaluated using the Shapiro–Wilk test, and the homogeneity of variance was assessed using Levene's test. Two-sample *t*-test or Wilcox test was used where appropriate. Chi-square tests were used to compare the difference in clinical features. Coefficients of correlation were computed using the Spearman's rank correlation method. Log-rank tests were used in survival analyses. Two-side *P* value less than 0.05 was considered statistically significant.

## Results

### The genetic and expression characteristics of ferroptosis-related genes in *EGFR/ALK*$^{WT}$ low-level PD-L1 NSCLC patients

In *EGFR/ALK*$^{WT}$ NSCLC patients with low-level PD-L1, missense mutation was the most frequent variant classification (Figure 2(A)). Single-nucleotide polymorphism (SNP) was the highest frequency variant type, while the most common single-nucleotide variant (SNV) class was C > A (Figure 2(B) and (C)). However, 71 of the 346 samples (20.52%) showed ferroptosis-related mutations (Figure 2(D)). Of these, *NFE2L2* exhibited the highest frequency of mutation (7%), followed by *DPP4* (4%). Interestingly, no *ATP5G3*, *LPCAT3*, *SAT1*, *CISD1*, *GPX4*, and *HSPB1* mutations were detected. The most commonly affected oncogenic pathway was the PTK-RAS pathway (78%), followed by the TP53 and Hippo pathways (62% and 59%, Figure 3). In total, 10 ferroptosis-related genes (*CDKN1A*, HSPA5, *NFE2L2*, *HSPB1*, *SLC1A5*, *TFRC*, *RPL8*, *LPCAT3*, *CS*, and *ATP5G3*) were upregulated in tumor samples compared to paracancer tissues, whereas 8 were downregulated (*GPX4*, *FANCD2*, *FDFT1*, *SAT1*, *NCOA4*, *DPP4*, *ALOX15*, and *ACSL4*) (Figure 4). To further study the interaction of ferroptosis-related genes, we used the STRING platform to conduct a PPI analysis and identified four genes as hub genes (*GPX4*, SLC7A11, *NFE2L2*, and *ACSL4*). The correlation network is represented in Figure 5(A) and (B).

### Identification of ferroptosis-related molecular subtypes

Based on the transcript levels of 24 ferroptosis regulators, we identified two different molecular patterns with the highest intragroup and low intergroup correlations using the unsupervised consensus clustering analysis (Figure 6(A), Supplementary Figures S1 and S2). Overall, 232 samples were assigned to the ferroptosis-related Cluster 1, while 119 were assigned to the ferroptosis-related Cluster 2. The ferroptosis regulators *SLC7A11*, *FANCD2*, *CISD1*, *TFRC*, *CARS*, and *ATP5G3* were significantly upregulated in Cluster 1, while *NFE2L2*, *HSPB1*, *GPX4*, *NCOA4*, *DPP4*, and *ALOX15* were downregulated (Supplementary Figure S3). Survival analysis demonstrated that ferroptosis-related Cluster 1 had a significantly better OS than Cluster 2 ($P = 0.004$, Figure 6(B)). We found that more males were in Cluster 1 ($P = 0.014$, Figure 7(A)), and patients were usually younger ($P = 0.011$, Figure 7(B)). No difference was detected between the two ferroptosis-related clusters in terms of pathological stage and type (Figure 7(C) and (D)). Using the significance criteria of $|\log2\text{-fold change}| > 0.8$ and FDR $< 0.05$, 169 DEGs were identified (Supplementary Table S2). Functional annotation-suggested DEGs were enriched in immune process pathways, including negative regulation of immune system process and humoral immune response (Figure 8). GSEA analysis revealed that the JAK-STAT, B cell receptor, chemokine, and T cell receptor signaling pathways were downregulated in Cluster 1 (Figure 9). In addition, the immune and stromal scores of Cluster 1 were significantly higher than that of Cluster 2 ($P < 0.001$ and $P < 0.01$, respectively, Figure 10(A) and (B)), while Cluster 1 had a higher tumor purity ($P < 0.001$, Figure 10(C)).

### Establishment and validation of a ferroptosis-related signature

To further explore the underlying association of ferroptosis-related clusters with prognosis, we developed a signature based on DEGs. To eliminate bias caused by non-tumor-related death, 11 samples having a median OS of fewer than 30 days or lacking survival data were excluded. Thus, 340 patients were randomly assigned to training and testing groups in a 7:3 ratio, resulting in 238 samples being assigned to the training group and 102 samples being assigned to the testing group. In the training group, univariate Cox regression analysis identified eight high-risky genes (*CPS1*, *STC2*, *INHA*, *HHIPL2*, *CAL*, *ABCC2*, *KLK8*, and *INSL4*) and six

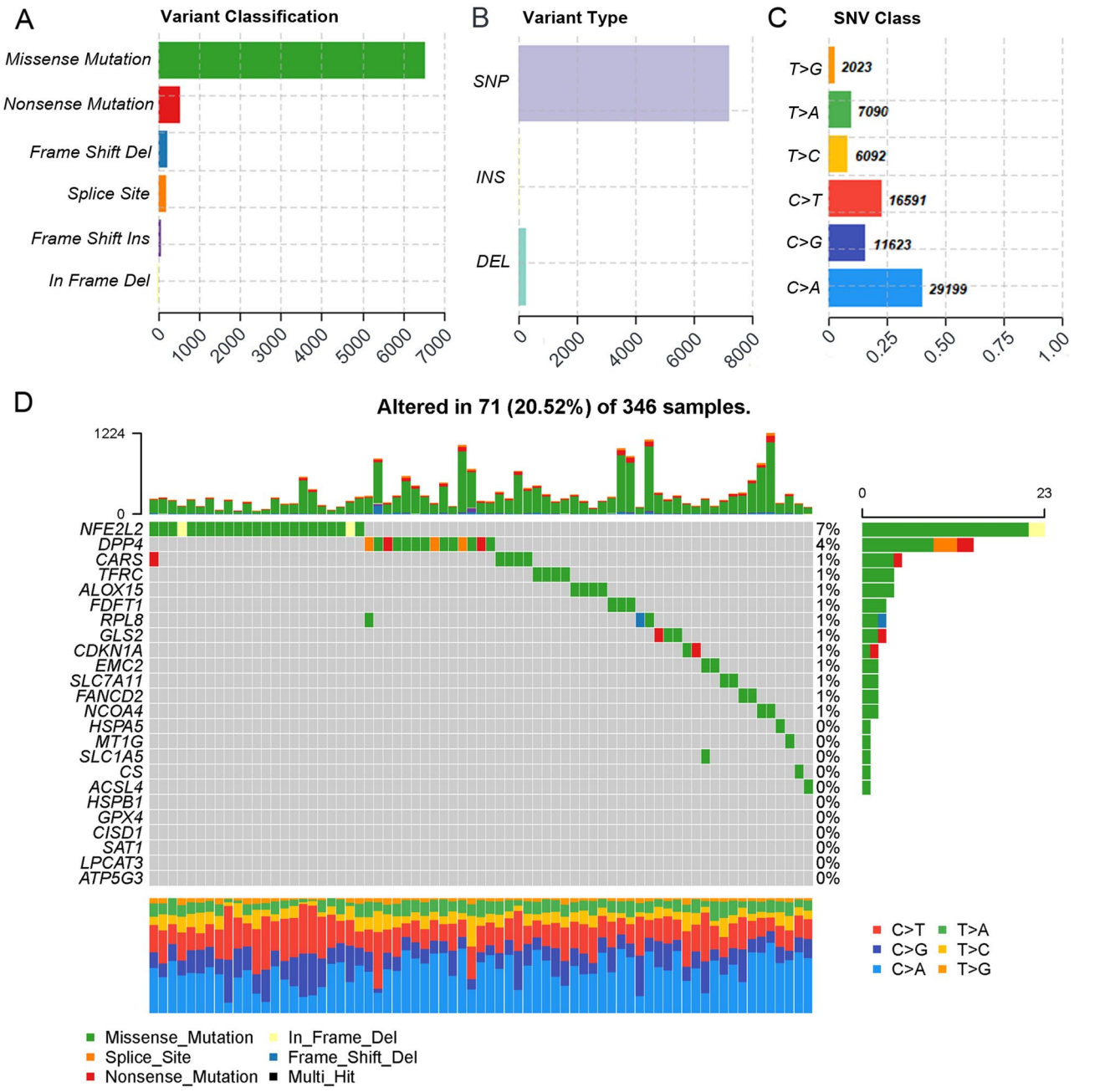


**Figure 2.** Genetic variation of ferroptosis-related genes in *EGFR/ALK*$^{WT}$ low-level PD-L1 NSCLC. The mutation frequency, classification, and waterfall plot based on 346 TCGA samples. (A color version of this figure is available in the online journal.)

protective genes (*CLIC6*, *SCL15A2*, *ADH1C*, *HLF*, and *CHST9*) using the criteria of $P < 0.05$ as cutoff (Supplementary Figure S4). Subsequently, LASSO regression narrowed down the potential markers, and an eight-gene ferroptosis-related signature was generated according to the minimum λ value (Supplementary Figures S5 and S6). Risk scores were calculated as follows: risk score = (−0.024**CLIC6*) + (−0.044**ADH1C*) + (0.023**CPS1*) + (0.018**STC2*) + (0.007**ABCC2*) + (0.041**KLK8*) + (0.067**INSL4*) + (−0.005**CHST9*) (Table 1).

According to the median score, 238 participants in the training cohort were divided into high- and low-risk subgroups. Survival analysis suggested that higher risk scores were associated with worse OS. The area under the curve (AUC) values for the signature were 0.672, 0.663, and 0.713 at 1, 3, and 5 years, respectively, according to the ROC curves (Figure 11(A) to (D)). The same formula was applied in the testing cohort and three independent validation sets, yielding similar results (Figure 11(E) to (H) and 12(A) to (C)), indicating a robust predictive performance of the ferroptosis-related signature model. In addition, the prognostic signature was better than other factors for predicting 5-year survival of NSCLC patients with *EGFR/ALK*$^{WT}$ and low-level PD-L1 (Figure 12(D)).

Univariate and multivariable regression analyses with the risk score and other clinical parameters were also performed. The univariate analysis suggested that increased risk scores

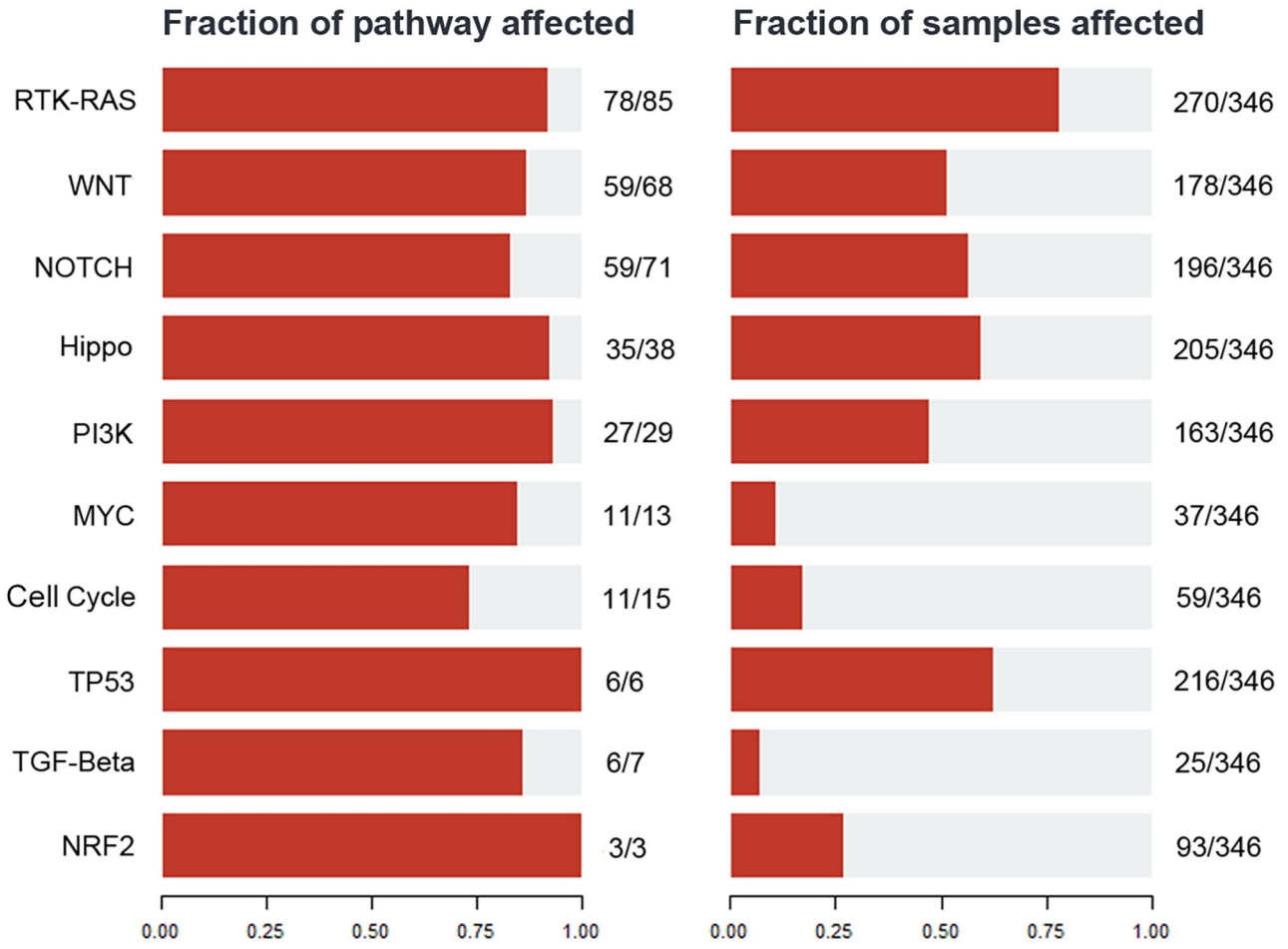


**Figure 3.** The mutation-affected carcinogenic pathways in *EGFR/ALK*$^{WT}$ low-level PD-L1 NSCLC. (A color version of this figure is available in the online journal.)

were significantly associated with poor prognosis (Figure 13(A)). In addition, the multivariate analysis suggested that the risk score might be used as an independent predictor of OS in *EGFR/ALK*$^{WT}$ low-level PD-L1 NSCLC patients (HR = 5.300, 95% CI: 2.701–10.404, Figure 13(B)).

### Immune cell infiltration analysis revealed an immune-suppressive state with higher risk scores

Based on currently accepted methodologies, the Spearman correlation of diverse immune cells with the risk score was estimated. As illustrated in Figure 14, negative correlation coefficients were frequently observed ($P < 0.05$), indicating an immune-excluded phenotype in individuals with a higher risk score. Most of the infiltrated cells were negatively associated with the risk score, consisting of both antitumor and immune-suppressive cells. For instance, all the immune infiltration prediction algorithms that indicated B cells were negatively linked to the risk score, and five algorithms identified a negative correlation between T cells and the risk score. In terms of immune-suppressive cells, a decreased number of myeloid dendritic cells and M2 macrophages was substantially associated with elevated risk scores as reported by more than four algorithms.

Along with the established cell infiltration algorithms, ssGSEA was also used to determine changes in immune function and pathways between low- and high-risk groups. Consistent with prior findings, significantly decreased ssGEEA scores were detected in a range of immune cell subsets (Figure 15(A)) and physiologic processes associated with the immune system (Figure 15(B)).

### The role of risk scores in immunotherapy response

Next, the potential connection between the risk score and response to ICIs was further evaluated. First, all samples were categorized into immunologically hot or cold tumors (Figure 16(A)), and we found that hot tumors had a significantly lower risk score ($P < 0.05$, Figure 16(B)). Furthermore, the IPS was calculated for different risk groups using TCIA, and the results indicated that patients in the low-risk group had a considerably greater IPS, implying a superior response to immunotherapy ($P < 0.01$, Figure 16(C)).

## Discussion

Among the 346 *EGFR/ALK*$^{WT}$ NSCLC patients with low PD-L1 expression, PTK-RAS pathways were the most

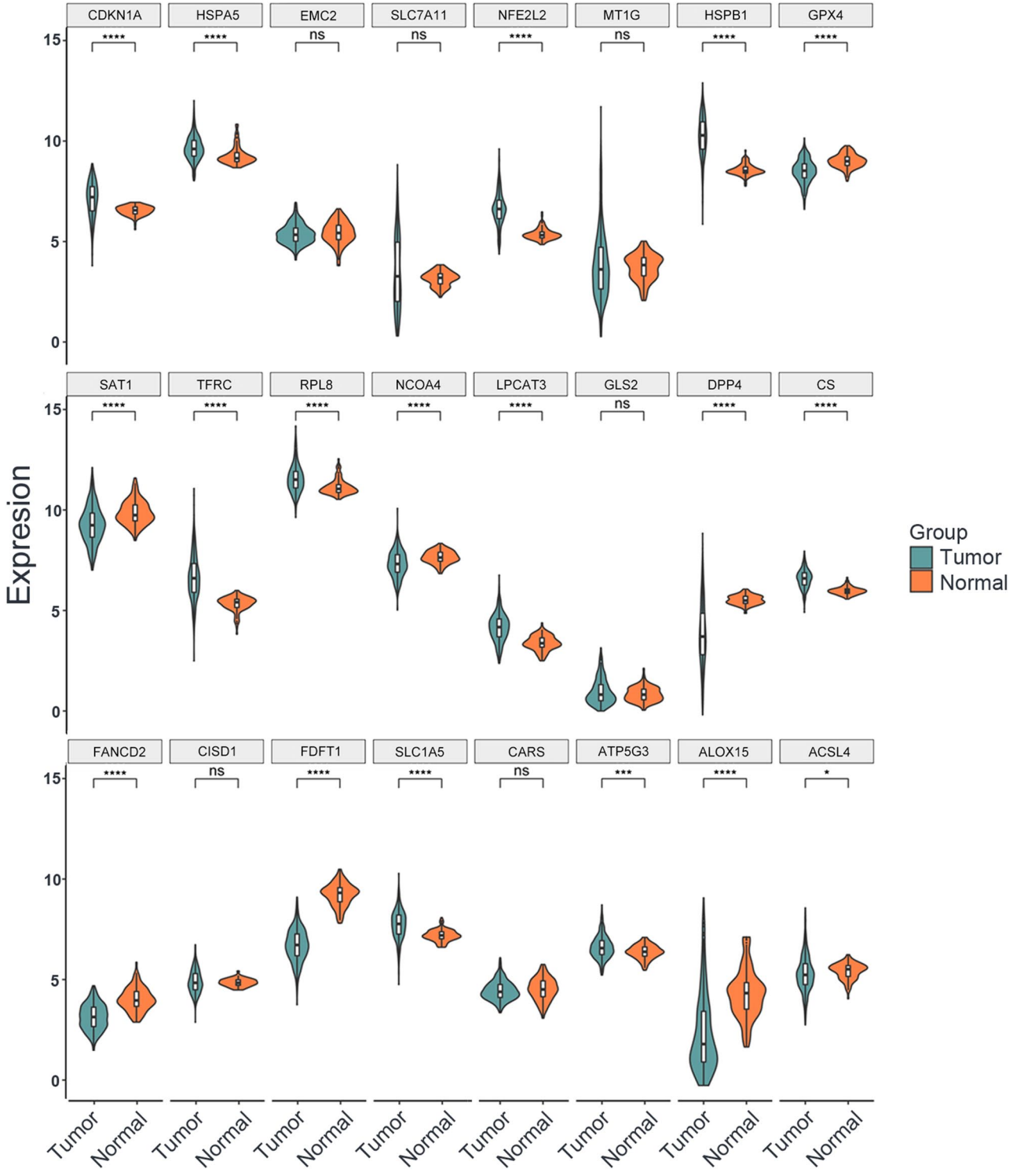


**Figure 4.** Transcript variation of ferroptosis-related genes in *EGFR*/*ALK*$^{WT}$ low-level PD-L1 NSCLC. The expression of 24 ferroptosis-related genes in *EGFR*/*ALK*$^{WT}$ and low PD-L1 expression NSCLC and paracancer tissues: tumor, atrovirens; and paracancer, orange. The boxes that represent median, interquartile range, and outliers are showed as black dots. Asterisks indicate statistical differences. (Wilcox test. ns means that $P \geqslant 0.05$; * means that $P < 0.05$; ** means that $P < 0.01$; *** means that $P < 0.001$). (A color version of this figure is available in the online journal.)

enriched carcinogenic signaling pathways. The activation of the RAS-RAF-MEK-ERK pathway has an indispensable effect on erastin-induced ferroptosis,[30] and *KAS* mutation predisposes lung adenocarcinoma to ferroptosis induced by SLC7A11 inhibitor.[31] Therefore, identifying the role of ferroptosis might help develop new strategies against *EGFR*/*ALK*$^{WT}$ NSCLC patients with negative PD-L1 expression.[32]

Given that ICIs and other therapies suppress cancer cells growth by inducing ferroptosis,[15,33] NSCLC patients with distinct ferroptosis patterns might have different prognoses

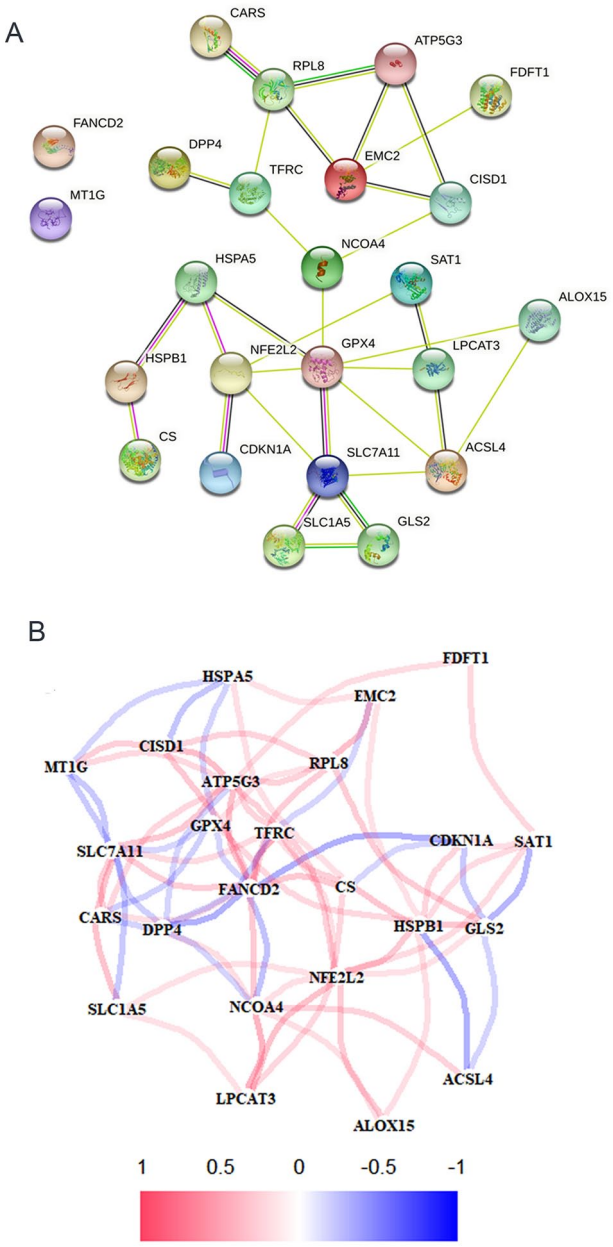


**Figure 5.** Network of ferroptosis-related genes. (A) PPI interactions network of ferroptosis-related genes (medium confidence = 0.4). (B) The correlation network of ferroptosis-related genes (red, positive correlation; blue, negative correlation; color depth represents the strength of the correlation). (A color version of this figure is available in the online journal.)

and immune phenotypes. In the current study, we generated a stable classification according to the expression of 24 ferroptosis-related genes. Remarkably, the two ferroptosis-related clusters revealed two distinct types of immune microenvironment state in *EGFR/ALK*$^{WT}$ low PD-L1 expression NSCLC patients, displaying significant differences in prognosis, biological functions, and immune cell infiltration. The ferroptosis-related Cluster 1 was characterized by survival disadvantage, high tumor purity, and low immune scores, whereas ferroptosis-related Cluster 2 showed better OS and higher immune scores. Functional enrichment analyses also showed a similar difference between the two clusters, in which immune-related pathways were significantly upregulated in Cluster 2. Taken together, these findings imply that distinct molecular patterns of ferroptosis may affect patient prognosis differently, presumably through the induction of distinct types of TIME.

A risk assessment model was developed based on two ferroptosis-related subtypes. Eight genes (*CLIC6*, *ADH1C*, *CHST9*, *CPS1*, *STC2*, *ABCC2*, *KLK8*, and *INSL4*) were identified for our prognostic signature, of which *CLIC6*, *ADH1C*, and *CHST9* were negatively associated with the risk score, while the other genes showed opposite correlations. *CLIC6* was first reported in rabbit gastric parietal cells.[34] Although its function is not completely clear, *CLIC6* has been shown to interact with dopamine receptors,[35] and its function may change according to lipids and oxidative conditions.[36] *ADH1C* encodes a Class I alcohol dehydrogenase and a

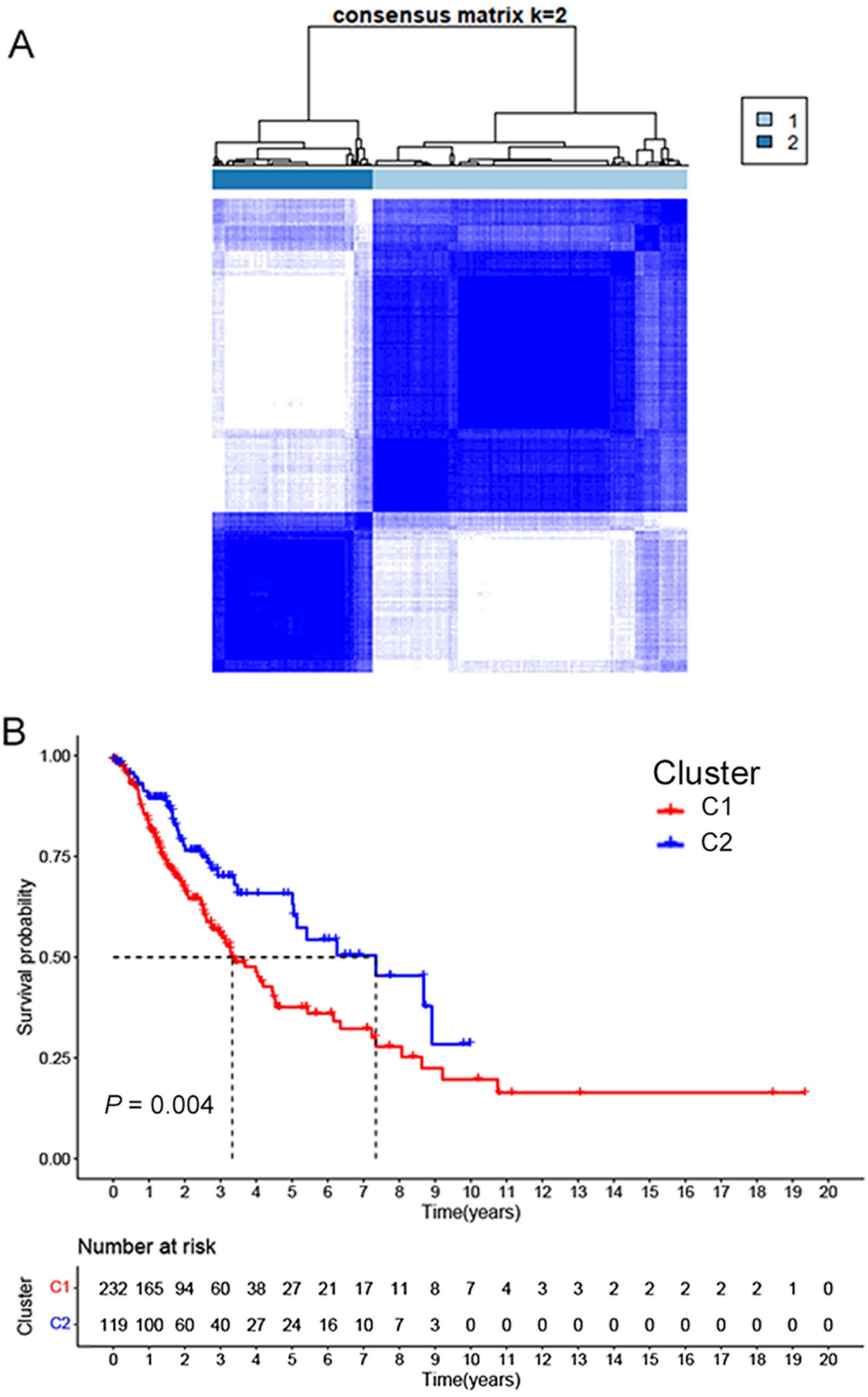


**Figure 6.** Subgroups of all samples associated with ferroptosis-related genes. (A) The consensus matrix with the highest intragroup and low intergroup correlations when $k=2$ in the training set. (B) Overall survival curves for the two ferroptosis-related clusters (log-rank test, $P=0.004$). (A color version of this figure is available in the online journal.)

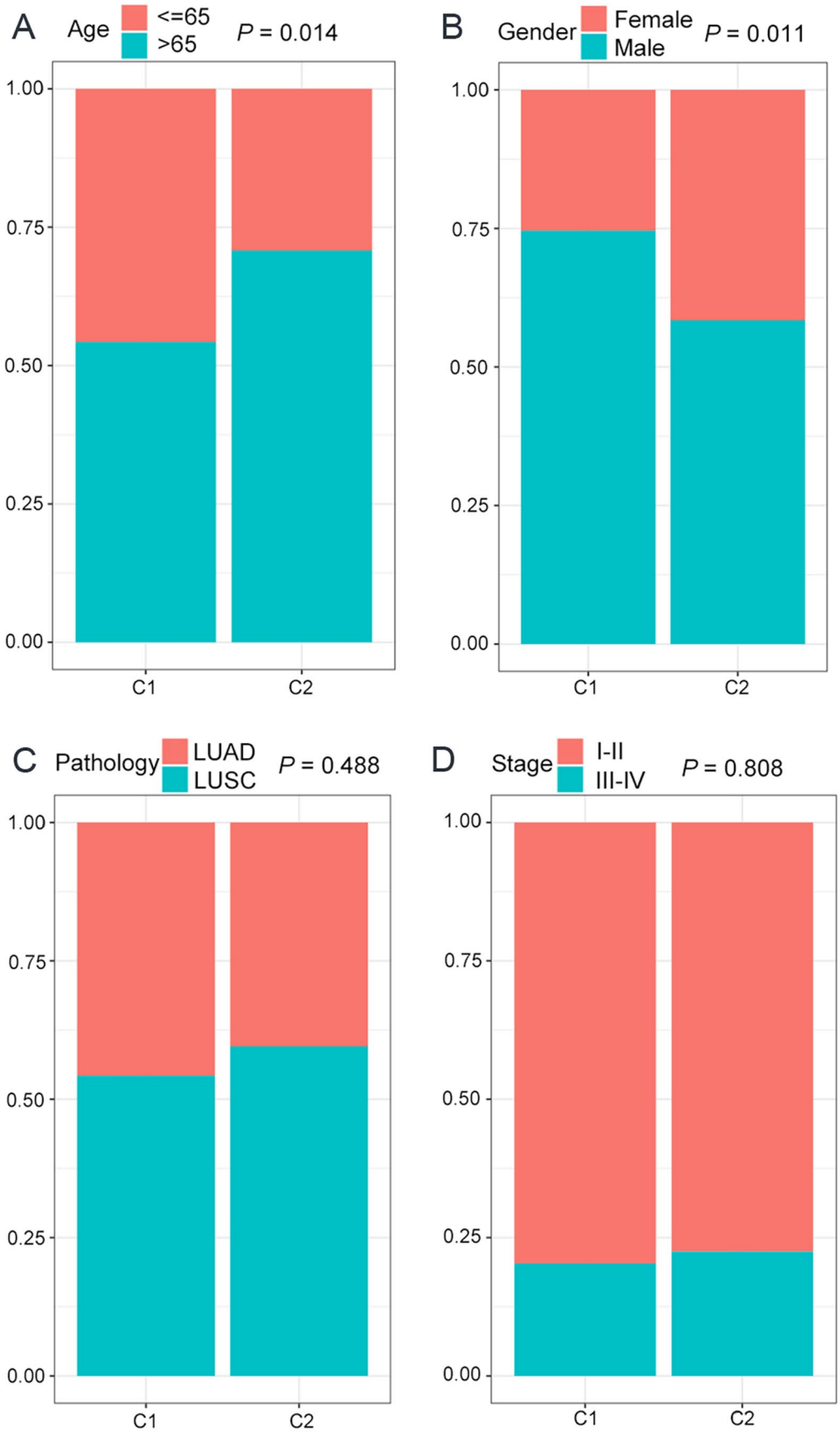


**Figure 7.** Clinical features of two clusters. Difference in age, gender, pathological stage, and pathological type between two ferroptosis-related clusters (Wilcox test). (A color version of this figure is available in the online journal.)

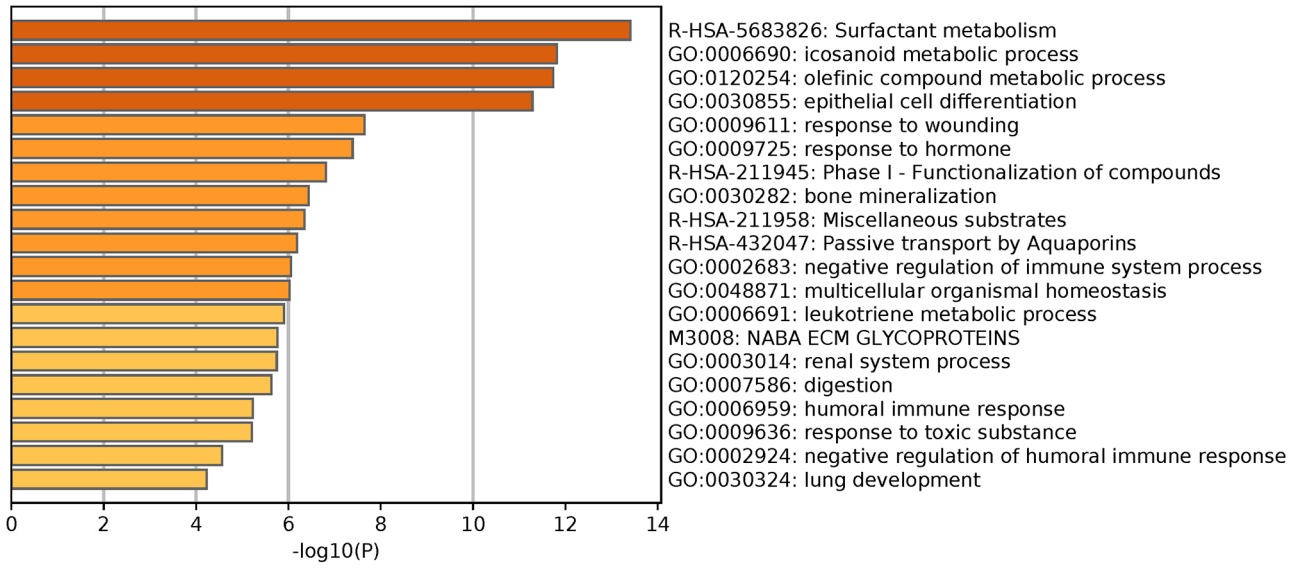


**Figure 8.** Functional annotation between subtypes. Bar graph of enriched terms across differential expression genes between two ferroptosis-related clusters, colored by *p*-values. (A color version of this figure is available in the online journal.)

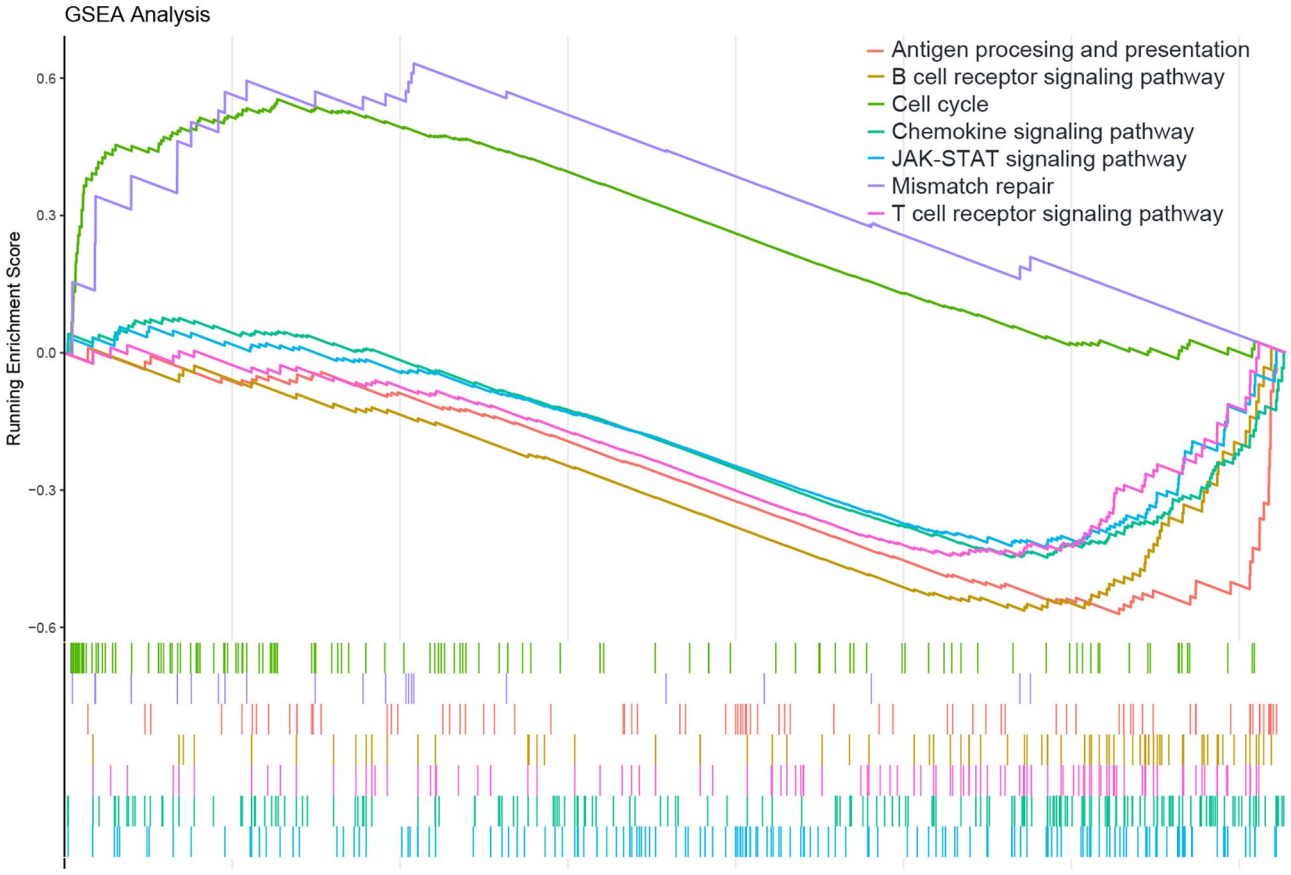


**Figure 9.** Gene set enrichment analysis. The enriched gene sets in KEGG. Left, Cluster 1; Right, Cluster 2. (A color version of this figure is available in the online journal.)

gamma subunit; it reportedly metabolizes various substrates, including lipid peroxidation products.[37] *CHST9* mediates sulfation of carbohydrate structures, which might be an alternative transsulfuration pathway to biosynthesize cysteine from methionine in tumor cells. *CPS1* can mediate the generation of carbamoyl phosphate in the mitochondria, which support the growth of *KRAS/LKB1*-mutant lung cancer cells.[38] *STC2* is involved in the growth, metastasis, and progression of lung cancer cells,[39] and overexpression of *STC2* can induce EGFR-TKI resistance through the

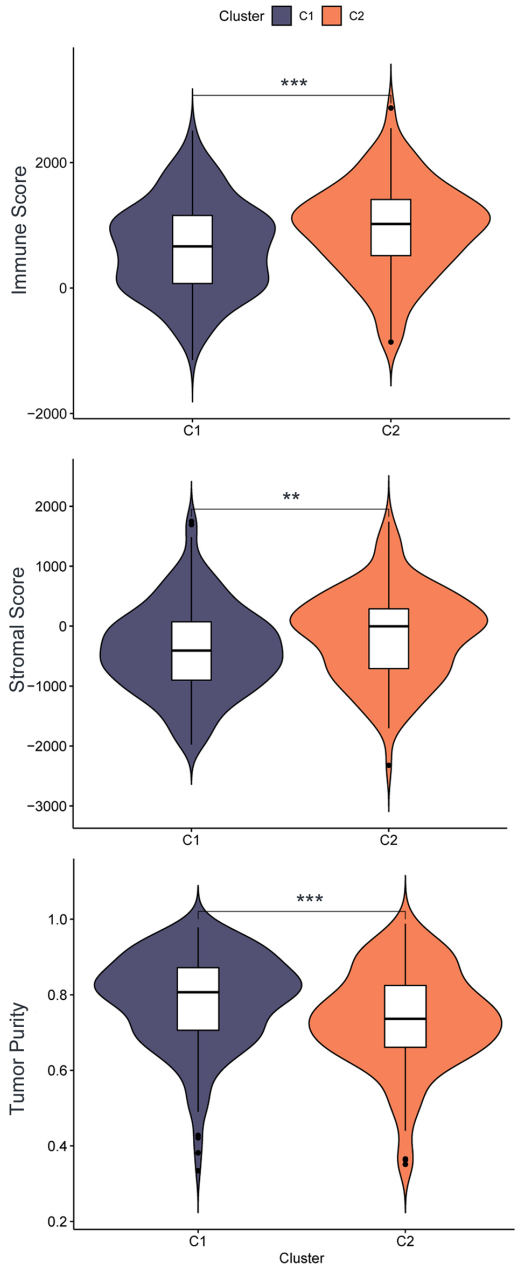


**Figure 10.** Estimation of immune, stromal score, and tumor purity. (A) Immune score in two ferroptosis-related clusters (*t*-test, ***$P < 0.001$). (B) and (C) Stromal score and tumor purity in two ferroptosis-related clusters (Wilcox test. **means that $P < 0.01$; *** means that $P < 0.001$.). (A color version of this figure is available in the online journal.)

STC2-JUN-AXL-ERK signaling pathway.[40] Previous studies have revealed that increased *ABCC2* expression was highly associated with platinum resistance,[41] making it a potential biomarker for NSCLC.[42] KLK8 is a favorable prognostic factor in ovarian cancer and lung cancer;[43,44] however, our signature model revealed that increased *KLK8* level was correlated with higher risk scores, implying a worse prognosis. *INSL4* showed an active tumor-promoting effect, and studies suggested that *INSL4* is a downstream molecular of *LKB1* inactivation and could promote proliferation, invasion, and migration of tumors.[45,46] The biological significance of *EGFR/ALK*$^{WT}$ and low PD-L1 expression in NSCLC has not been widely addressed. Altogether, our signature demonstrated robust performance in predicting prognosis, indicating that each gene deserves further study in future research.

Based on the results of multicenter randomized controlled trials,[47,48] a relatively small subset of NSCLC patients who do not express PD-L1 might also benefit from a durable response to ICIs. Therefore, identifying this subgroup of patients has important biological and clinical implications. The TIME state is critical in determining prognosis and treatment response. Previous studies have put forward various classification schemes based on their TIME state, such as hot or cold tumors,[27] immune-inflamed, immune-excluded, or immune-desert tumors.[49] Generally, abundant infiltration of anticancer immune cells is more likely, but not always, linked to better prognosis and response to ICIs. The current study found that the risk score may serve as an independent predictor for ICIs response, where higher risk scores indicate poor response to ICIs.[50] First, most of the immune cells, both immune-activating and immune-suppressing cells, were reduced as the risk score increased, indicating an immune-excluded or immune-desert phenotype. Second, after classifying all samples into cold or hot tumors, we noted that cold tumors have significantly higher risk scores. Finally, significantly lower IPSs were found in the high-risk group.

In conclusion, ferroptosis regulators play a critical role in determining the risk of *EGFR/ALK*$^{WT}$ NSCLC patients with low PD-L1 expression. The high-risk patients presented with a worse OS and response to ICIs, which was possibly induced by negative TIME modulation. The current study advances our understanding of ferroptosis in NSCLC patients and lays a foundation for developing novel therapeutic strategies.

**Table 1.** Ferroptosis-related signature score and coefficients.

| Gene symbol | Description | Coefficient |
|---|---|---|
| CLIC6 | Chloride intracellular channel 6 | −0.024 |
| ADH1C | Alcohol dehydrogenase 1C | −0.044 |
| CHST9 | Carbohydrate sulfotransferase 9 | −0.005 |
| CPS1 | Carbamoyl-phosphate synthase | 0.023 |
| STC2 | Stanniocalcin-2 | 0.018 |
| ABCC2 | ATP-binding cassette sub-family C member 2 | 0.007 |
| KLK8 | Kallikrein-8 | 0.041 |
| INSL4 | Early placenta insulin-like peptide | 0.067 |

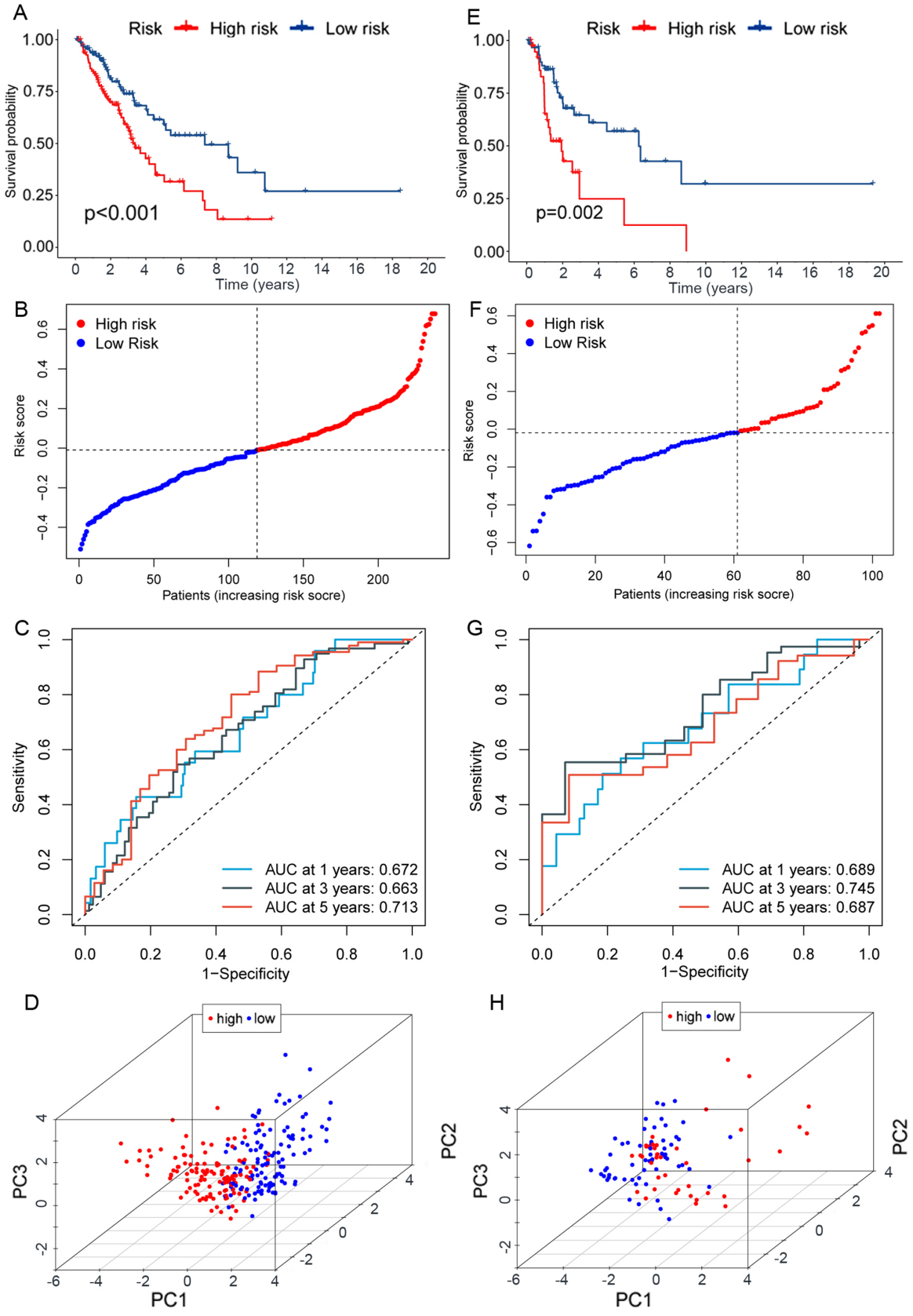


**Figure 11.** Construction and validation of the ferroptosis-related model. (A) Kaplan–Meier curves for OS according to ferroptosis-related risk groups in the training set (log-rank test). (B) Distribution of risk scores of the ferroptosis-related signature in the training set. (C) ROC curves of the risk score in the training set. (D) The PCA analysis of ferroptosis-related risk groups. (E) to (H) Validation in the testing set. (A color version of this figure is available in the online journal.)

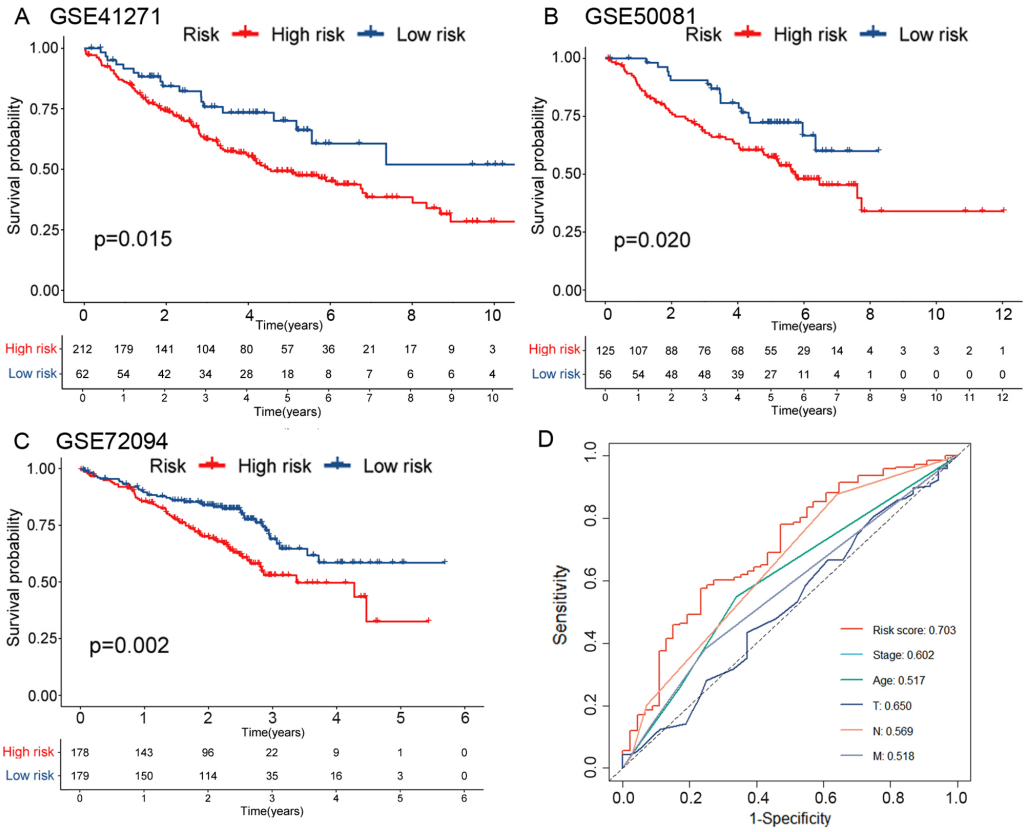


**Figure 12.** External validation of the ferroptosis-related model. (A) to (C) External validation of the model based on three independent sets (GSE72094, GSE41271, and GSE50081). (D) ROC curves about the risk score, age, pathological stage, T, M, and N stage in TCGA cohorts. (A color version of this figure is available in the online journal.)

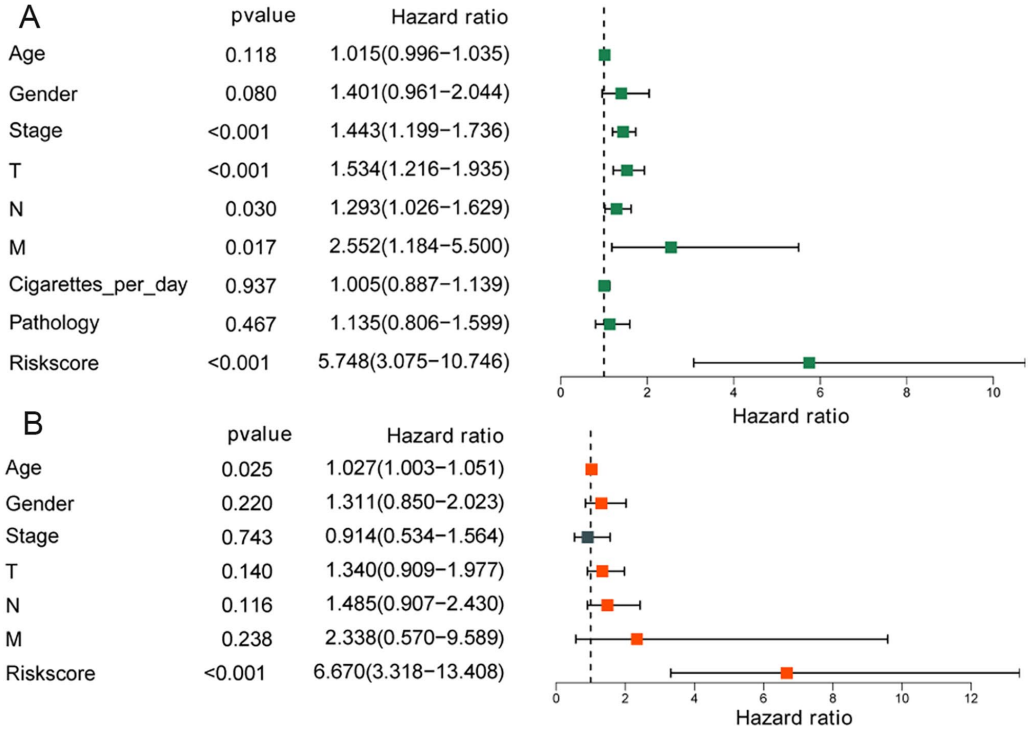


**Figure 13.** Cox regression analysis of the risk score. (A) and (B) Univariate and multivariate Cox regression of OS in the TCGA cohort. (A color version of this figure is available in the online journal.)

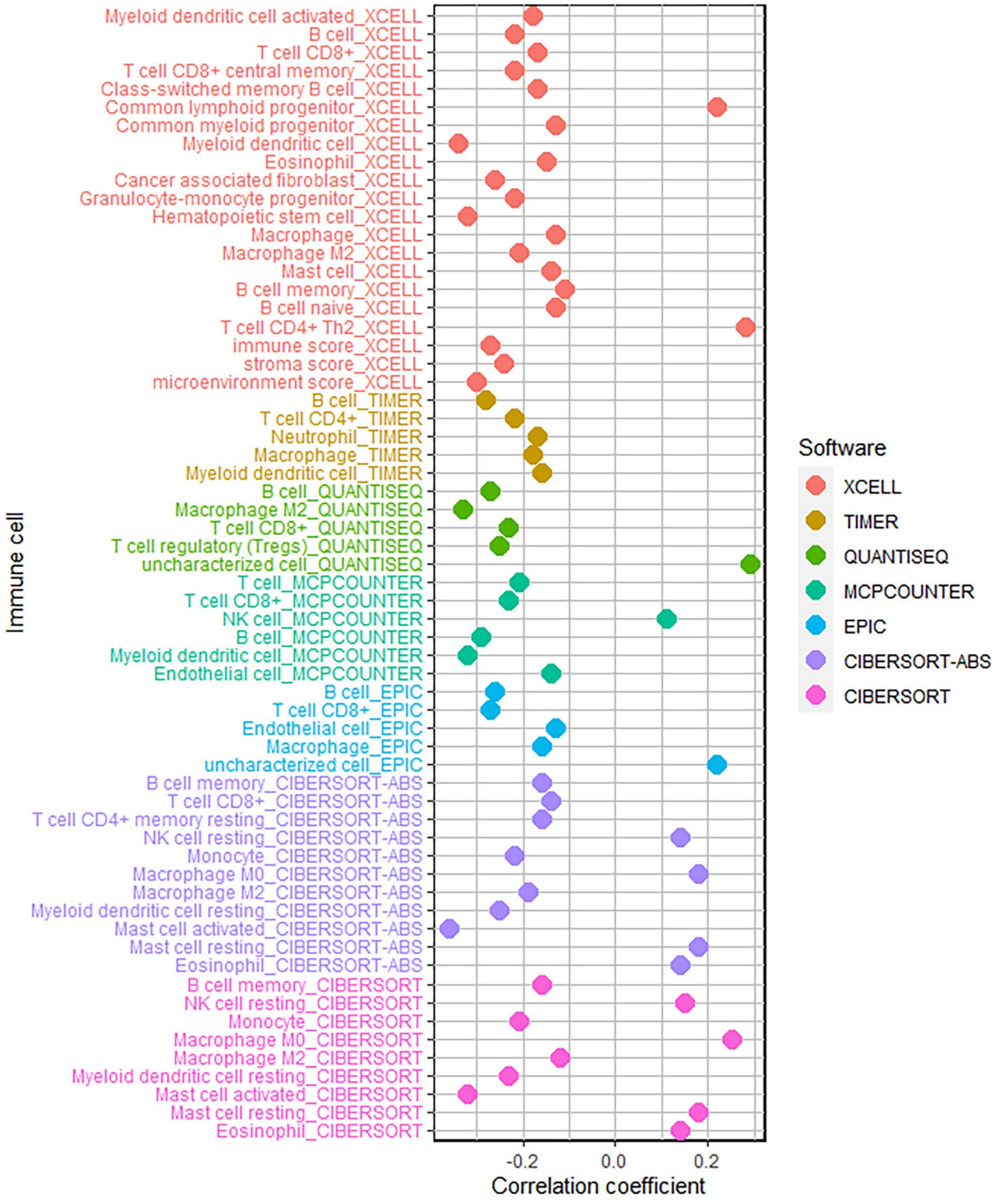


**Figure 14.** Immune cell infiltration analysis related to the risk score. Correlation of the risk score with estimated tumor-infiltrated immune cells. (A color version of this figure is available in the online journal.)

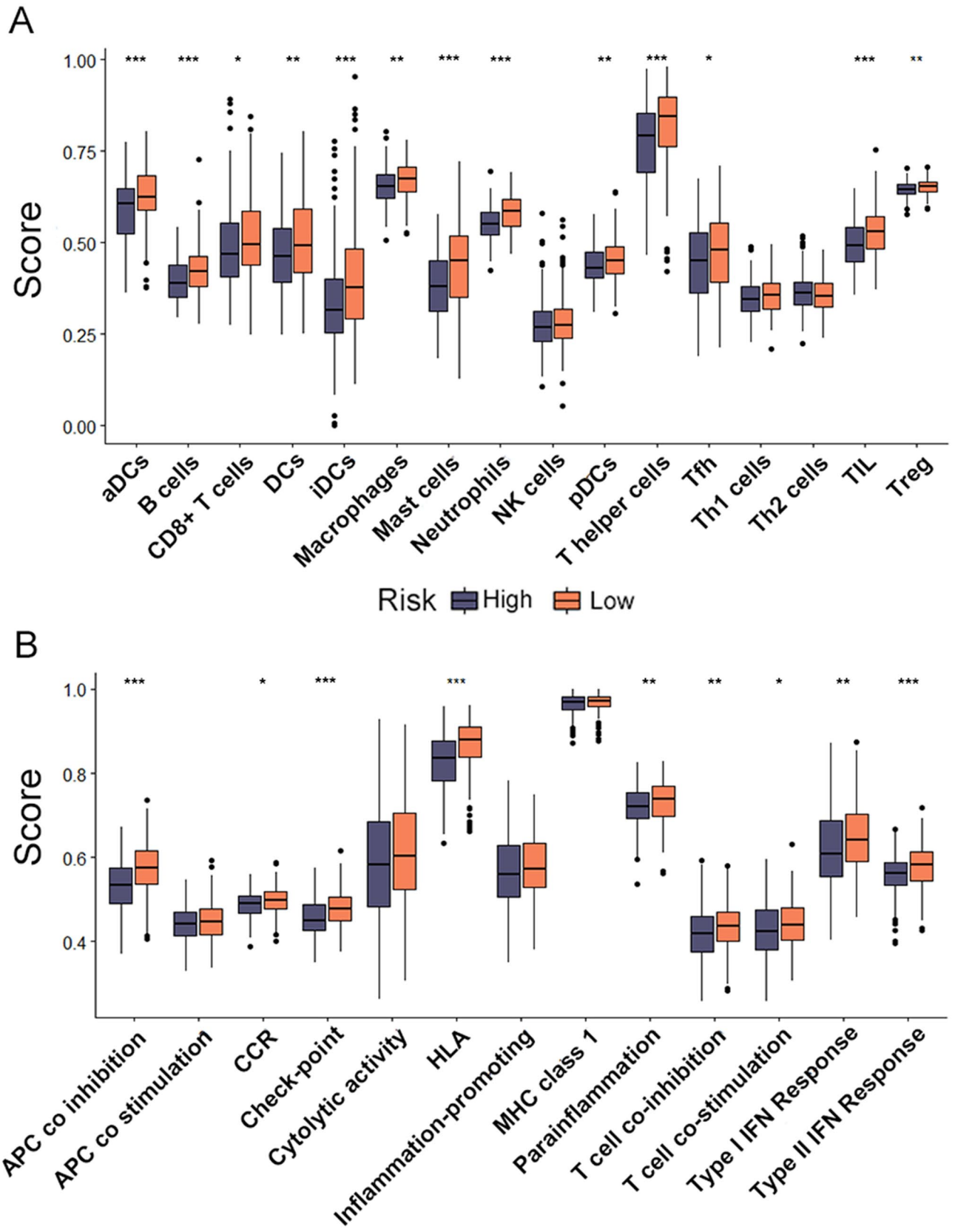


**Figure 15.** Immune cell infiltration analysis between high- and low-risk groups. (A) and (B) Differences in the ssGSEA scores based on 29 immune-related gene sets between low- (orange) and high-risk (navy blue) group (Wilcox test). (A color version of this figure is available in the online journal.)

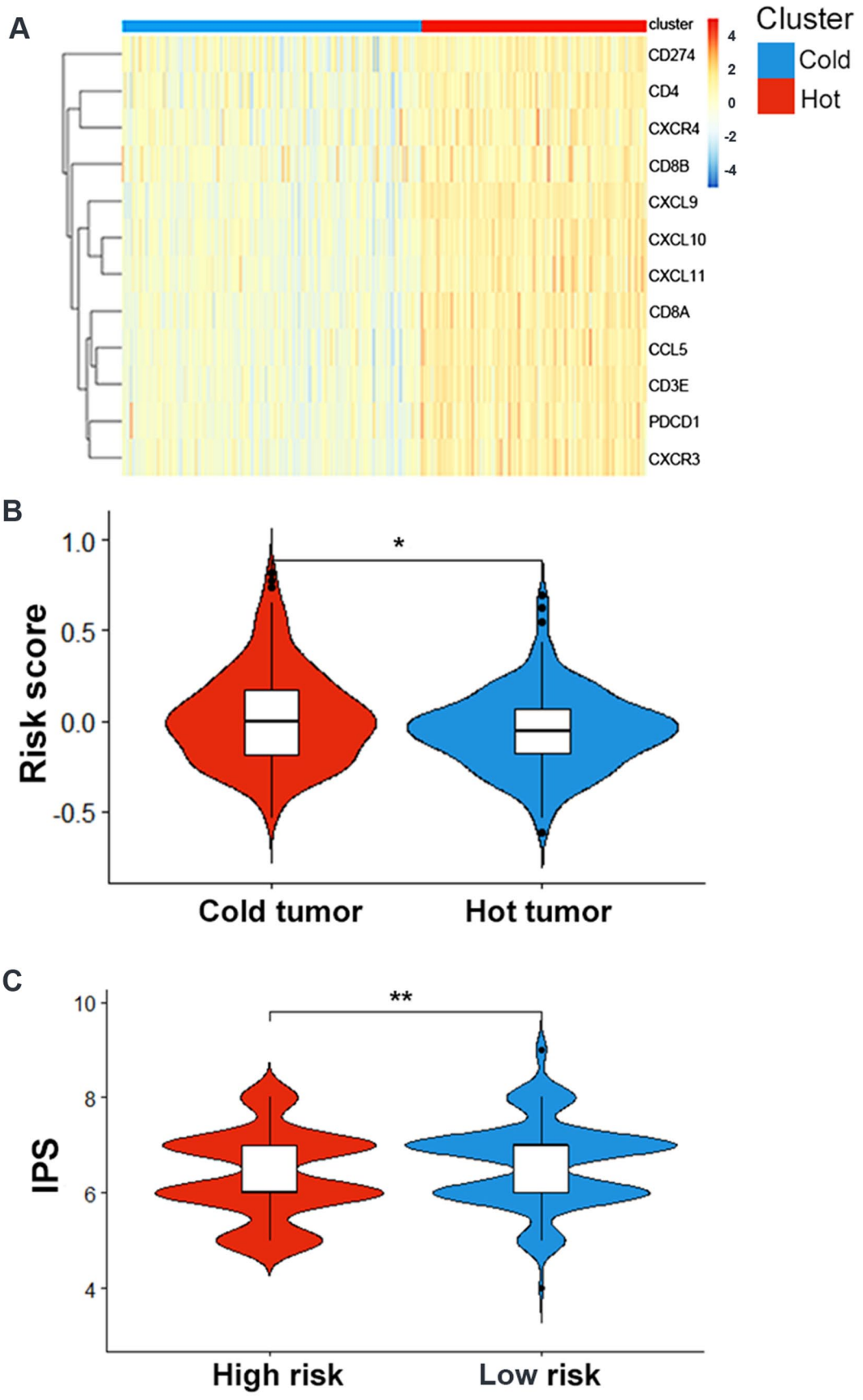


**Figure 16.** Immunotherapy response analyses. (A) Heatmap plot of hot or cold tumor markers. (B) Violin plot of risk scores in hot or cold tumors. (C) Violin plot of IPS in low- and high-risk groups. (A color version of this figure is available in the online journal.)

## AUTHORS' CONTRIBUTIONS

H-BZ and Y-JZ were responsible for the conception of this study. RZ and H-CM drafted and wrote the manuscript. Y-HL and XC made critical review and commentary on this manuscript. RZ, X-SC, and Y-DC acquired and analyzed the data. L-RL and YL searched the related studies and provided critical progress on ferroptosis. All the authors reviewed the final manuscript and agreed to the submission. RZ, H-CM, Y-HL, and XC contributed equally to this work.

## DECLARATION OF CONFLICTING INTERESTS

The author(s) declared no potential conflicts of interest with respect to the research, authorship, and/or publication of this article.

## FUNDING

The author(s) disclosed receipt of the following financial support for the research, authorship, and/or publication of this article: This work was supported by the Science and Technology Planning Project of Guangdong Province (No. 2017B030314166) and the 2020 Guangdong Provincial Science and Technology Innovation Strategy Special Fund (Guangdong-Hong Kong-Macau Joint Lab, No: 2020B1212030006).

## DATA AVAILABILITY

All data analyzed in this study were available from publicly online databases (TCGA and GEO). Information about each dataset was presented in the manuscript.

## ORCID ID

Rui Zhou https://orcid.org/0000-0003-2315-5569

## SUPPLEMENTAL MATERIAL

Supplemental material for this article is available online.

## REFERENCES

1. Sung H, Ferlay J, Siegel RL, Laversanne M, Soerjomataram I, Jemal A, Bray F. Global Cancer Statistics 2020: GLOBOCAN estimates of incidence and mortality worldwide for 36 cancers in 185 countries. *CA Cancer J Clin* 2021;**71**:209–49
2. Proto C, Lo Russo G, Corrao G, Ganzinelli M, Facchinetti F, Minari R, Tiseo M, Garassino MC. Treatment in EGFR-mutated non-small cell lung cancer: how to block the receptor and overcome resistance mechanisms. *Tumori* 2017;**103**:325–37
3. Zhong WZ, Zhou Q, Wu YL. The resistance mechanisms and treatment strategies for EGFR-mutant advanced non-small-cell lung cancer. *Oncotarget* 2017;**8**:71358–70
4. Carbone DP, Reck M, Paz-Ares L, Creelan B, Horn L, Steins M, Felip E, van den Heuvel MM, Ciuleanu TE, Badin F, Ready N, Hiltermann TJN, Nair S, Juergens R, Peters S, Minenza E, Wrangle JM, Rodriguez-Abreu D, Borghaei H, Blumenschein GR Jr, Villaruz LC, Havel L, Krejci J, Corral Jaime J, Chang H, Geese WJ, Bhagavatheeswaran P, Chen AC, Socinski MA. First-line nivolumab in stage IV or recurrent non-small-cell lung cancer. *N Engl J Med* 2017;**376**:2415–26
5. Gandhi L, Rodríguez-Abreu D, Gadgeel S, Esteban E, Felip E, De Angelis F, Domine M, Clingan P, Hochmair MJ, Powell SF, Cheng SY, Bischoff HG, Peled N, Grossi F, Jennens RR, Reck M, Hui R, Garon EB, Boyer M, Rubio-Viqueira B, Novello S, Kurata T, Gray JE, Vida J, Wei Z, Yang J, Raftopoulos H, Pietanza MC, Garassino MC. Pembrolizumab plus chemotherapy in metastatic non-small-cell lung cancer. *N Engl J Med* 2018;**378**:2078–92
6. Garassino MC, Gadgeel S, Esteban E, Felip E, Speranza G, Domine M, Hochmair MJ, Powell S, Cheng SY, Bischoff HG, Peled N, Reck M, Hui R, Garon EB, Boyer M, Wei Z, Burke T, Pietanza MC, Rodríguez-Abreu D. Patient-reported outcomes following pembrolizumab or placebo plus pemetrexed and platinum in patients with previously untreated, metastatic, non-squamous non-small-cell lung cancer (KEYNOTE-189): a multicentre, double-blind, randomised, placebo-controlled, phase 3 trial. *Lancet Oncol* 2020;**21**:387–97
7. West H, McCleod M, Hussein M, Morabito A, Rittmeyer A, Conter HJ, Kopp HG, Daniel D, McCune S, Mekhail T, Zer A, Reinmuth N, Sadiq A, Sandler A, Lin W, Ochi Lohmann T, Archer V, Wang L, Kowanetz M, Cappuzzo F. Atezolizumab in combination with carboplatin plus nab-paclitaxel chemotherapy compared with chemotherapy alone as first-line treatment for metastatic non-squamous non-small-cell lung cancer (IMpower130): a multicentre, randomised, open-label, phase 3 trial. *Lancet Oncol* 2019;**20**:924–37
8. Langer CJ, Gadgeel SM, Borghaei H, Papadimitrakopoulou VA, Patnaik A, Powell SF, Gentzler RD, Martins RG, Stevenson JP, Jalal SI, Panwalkar A, Yang JC, Gubens M, Sequist LV, Awad MM, Fiore J, Ge Y, Raftopoulos H, Gandhi L. Carboplatin and pemetrexed with or without pembrolizumab for advanced, non-squamous non-small-cell lung cancer: a randomised, phase 2 cohort of the open-label KEYNOTE-021 study. *Lancet Oncol* 2016;**17**:1497–508
9. Paz-Ares L, Vicente D, Tafreshi A, Robinson A, Soto Parra H, Mazières J, Hermes B, Cicin I, Medgyasszay B, Rodríguez-Cid J, Okamoto I, Lee S, Ramlau R, Vladimirov V, Cheng Y, Deng X, Zhang Y, Bas T, Piperdi B, Halmos B. A Randomized, placebo-controlled trial of pembrolizumab plus chemotherapy in patients with metastatic squamous NSCLC: protocol-specified final analysis of KEYNOTE-407. *J Thorac Oncol* 2020;**15**:1657–69
10. Dixon SJ, Lemberg KM, Lamprecht MR, Skouta R, Zaitsev EM, Gleason CE, Patel DN, Bauer AJ, Cantley AM, Yang WS, Morrison B, 3rd Stockwell BR. Ferroptosis: an iron-dependent form of nonapoptotic cell death. *Cell* 2012;**149**:1060–72
11. Stockwell BR, Friedmann Angeli JP, Bayir H, Bush AI, Conrad M, Dixon SJ, Fulda S, Gascón S, Hatzios SK, Kagan VE, Noel K, Jiang X, Linkermann A, Murphy ME, Overholtzer M, Oyagi A, Pagnussat GC, Park J, Ran Q, Rosenfeld CS, Salnikow K, Tang D, Torti FM, Torti SV, Toyokuni S, Woerpel KA, Zhang DD. Ferroptosis: a regulated cell death nexus linking metabolism, redox biology, and disease. *Cell* 2017;**171**:273–85
12. Yang WS, Stockwell BR. Synthetic lethal screening identifies compounds activating iron-dependent, nonapoptotic cell death in oncogenic-RAS-harboring cancer cells. *Chem Biol* 2008;**15**:234–45
13. Hassannia B, Vandenabeele P, Vanden Berghe T. Targeting ferroptosis to iron out cancer. *Cancer Cell* 2019;**35**:830–49
14. Viswanathan VS, Ryan MJ, Dhruv HD, Gill S, Eichhoff OM, Seashore-Ludlow B, Kaffenberger SD, Eaton JK, Shimada K, Aguirre AJ, Viswanathan SR, Chattopadhyay S, Tamayo P, Yang WS, Rees MG, Chen S, Boskovic ZV, Javaid S, Huang C, Wu X, Tseng YY, Roider EM, Gao D, Cleary JM, Wolpin BM, Mesirov JP, Haber DA, Engelman JA, Boehm JS, Kotz JD, Hon CS, Chen Y, Hahn WC, Levesque MP, Doench JG, Berens ME, Shamji AF, Clemons PA, Stockwell BR, Schreiber SL. Dependency of a therapy-resistant state of cancer cells on a lipid peroxidase pathway. *Nature* 2017;**547**:453–7
15. Wang W, Green M, Choi JE, Gijón M, Kennedy PD, Johnson JK, Liao P, Lang X, Kryczek I, Sell A, Xia H, Zhou J, Li G, Li J, Li W, Wei S, Vatan L, Zhang H, Szeliga W, Gu W, Liu R, Lawrence TS, Lamb C, Tanno Y, Cieslik M, Stone E, Georgiou G, Chan TA, Chinnaiyan A, Zou W. CD8(+) T cells regulate tumour ferroptosis during cancer immunotherapy. *Nature* 2019;**569**:270–4
16. Wen Q, Liu J, Kang R, Zhou B, Tang D. The release and activity of HMGB1 in ferroptosis. *Biochem Biophys Res Commun* 2019;**510**:278–83
17. Dai E, Han L, Liu J, Xie Y, Kroemer G, Klionsky DJ, Zeh HJ, Kang R, Wang J, Tang D. Autophagy-dependent ferroptosis drives tumor-associated macrophage polarization via release and uptake of oncogenic KRAS protein. *Autophagy* 2020;**16**:2069–83
18. Ritchie ME, Phipson B, Wu D, Hu Y, Law CW, Shi W, Smyth GK. limma powers differential expression analyses for RNA-sequencing and microarray studies. *Nucleic Acids Res* 2015;**43**:e47

19. Mayakonda A, Lin DC, Assenov Y, Plass C, Koeffler HP. Maftools: efficient and comprehensive analysis of somatic variants in cancer. *Genome Res* 2018;**28**:1747–56
20. Mora A, Donaldson IM. iRefR: an R package to manipulate the iRefIndex consolidated protein interaction database. *BMC Bioinformatics* 2011;**12**:455
21. Wilkerson MD, Hayes DN. ConsensusClusterPlus: a class discovery tool with confidence assessments and item tracking. *Bioinformatics* 2010;**26**:1572–3
22. Hartigan J, Wong M. Algorithm AS 136: a K-means clustering algorithm. *Journal of the Royal Statistical Society* 1979;**28**:100–8
23. Friedman J, Hastie T, Tibshirani R. Regularization paths for generalized linear models via coordinate descent. *J Stat Softw* 2010;**33**:1–22
24. Heagerty PJ, Zheng Y. Survival model predictive accuracy and ROC curves. *Biometrics* 2005;**61**:92–105
25. Yoshihara K, Shahmoradgoli M, Martínez E, Vegesna R, Kim H, Torres-Garcia W, Treviño V, Shen H, Laird PW, Levine DA, Carter SL, Getz G, Stemke-Hale K, Mills GB, Verhaak RG. Inferring tumour purity and stromal and immune cell admixture from expression data. *Nat Commun* 2013;**4**:2612
26. Angelova M, Charoentong P, Hackl H, Fischer ML, Snajder R, Krogsdam AM, Waldner MJ, Bindea G, Mlecnik B, Galon J, Trajanoski Z. Characterization of the immunophenotypes and antigenomes of colorectal cancers reveals distinct tumor escape mechanisms and novel targets for immunotherapy. *Genome Biol* 2015;**16**:64
27. Bonaventura P, Shekarian T, Alcazer V, Valladeau-Guilemond J, Valsesia-Wittmann S, Amigorena S, Caux C, Depil S. Cold tumors: a therapeutic challenge for immunotherapy. *Front Immunol* 2019;**10**:168
28. Charoentong P, Finotello F, Angelova M, Mayer C, Efremova M, Rieder D, Hackl H, Trajanoski Z. Pan-cancer immunogenomic analyses reveal genotype-immunophenotype relationships and predictors of response to checkpoint blockade. *Cell Rep* 2017;**18**:248–62
29. Clyde D. Cancer genomics: keeping score with immunotherapy response. *Nat Rev Genet* 2017;**18**:146
30. Yagoda N, von Rechenberg M, Zaganjor E, Bauer AJ, Yang WS, Fridman DJ, Wolpaw AJ, Smukste I, Peltier JM, Boniface JJ, Smith R, Lessnick SL, Sahasrabudhe S, Stockwell BR. RAS-RAF-MEK-dependent oxidative cell death involving voltage-dependent anion channels. *Nature* 2007;**447**:864–8
31. Hu K, Li K, Lv J, Feng J, Chen J, Wu H, Cheng F, Jiang W, Wang J, Pei H, Chiao PJ, Cai Z, Chen Y, Liu M, Pang X. Suppression of the SLC7A11/glutathione axis causes synthetic lethality in KRAS-mutant lung adenocarcinoma. *J Clin Invest* 2020;**130**:1752–66
32. Chen X, Kang R, Kroemer G, Tang D. Broadening horizons: the role of ferroptosis in cancer. *Nat Rev Clin Oncol* 2021;**18**:280–96
33. Kuang Y, Wang Q. Iron and lung cancer. *Cancer Lett* 2019;**464**:56–61
34. Nishizawa T, Nagao T, Iwatsubo T, Forte JG, Urushidani T. Molecular cloning and characterization of a novel chloride intracellular channel-related protein, parchorin, expressed in water-secreting cells. *J Biol Chem* 2000;**275**:11164–73
35. Griffon N, Jeanneteau F, Prieur F, Diaz J, Sokoloff P. CLIC6, a member of the intracellular chloride channel family, interacts with dopamine D(2)-like receptors. *Brain Res Mol Brain Res* 2003;**117**:47–57
36. Ferofontov A, Strulovich R, Marom M, Giladi M, Haitin Y. Inherent flexibility of CLIC6 revealed by crystallographic and solution studies. *Sci Rep* 2018;**8**:6882
37. Furuhashi T, Ishii R, Onishi H, Ota S. Elucidation of biochemical pathways underlying VOCs production in A549 cells. *Front Mol Biosci* 2020;**7**:116
38. Kim J, Hu Z, Cai L, Li K, Choi E, Faubert B, Bezwada D, Rodriguez-Canales J, Villalobos P, Lin YF, Ni M, Huffman KE, Girard L, Byers LA, Unsal-Kacmaz K, Peña CG, Heymach JV, Wauters E, Vansteenkiste J, Castrillon DH, Chen BPC, Wistuba I, Lambrechts D, Xu J, Minna JD, DeBerardinis RJ. CPS1 maintains pyrimidine pools and DNA synthesis in KRAS/LKB1-mutant lung cancer cells. *Nature* 2017;**546**:168–72
39. Na SS, Aldonza MB, Sung HJ, Kim YI, Son YS, Cho S, Cho JY. Stanniocalcin-2 (STC2): a potential lung cancer biomarker promotes lung cancer metastasis and progression. *Biochim Biophys Acta* 2015; **1854**:668–76
40. Liu YN, Tsai MF, Wu SG, Chang TH, Tsai TH, Gow CH, Chang YL, Shih JY. Acquired resistance to EGFR tyrosine kinase inhibitors is mediated by the reactivation of STC2/JUN/AXL signaling in lung cancer. *Int J Cancer* 2019;**145**:1609–24
41. Cuffe S, Azad AK, Qiu X, Qiu X, Brhane Y, Kuang Q, Marsh S, Savas S, Chen Z, Cheng D, Leighl NB, Goss G, Laurie SA, Seymour L, Bradbury PA, Shepherd FA, Tsao MS, Chen BE, Xu W, Liu G. ABCC2 polymorphisms and survival in the Princess Margaret cohort study and the NCIC clinical trials group BR.24 trial of platinum-treated advanced stage non-small cell lung cancer patients. *Cancer Epidemiol* 2016;**41**:50–6
42. Chen Y, Zhou H, Yang S, Su D. Increased ABCC2 expression predicts cisplatin resistance in non-small cell lung cancer. *Cell Biochem Funct* 2021;**39**:277–86
43. Borgoño CA, Kishi T, Scorilas A, Harbeck N, Dorn J, Schmalfeldt B, Schmitt M, Diamandis EP. Human kallikrein 8 protein is a favorable prognostic marker in ovarian cancer. *Clin Cancer Res* 2006;**12**:1487–93
44. Sher YP, Chou CC, Chou RH, Wu HM, Wayne Chang WS, Chen CH, Yang PC, Wu CW, Yu CL, Peck K. Human kallikrein 8 protease confers a favorable clinical outcome in non-small cell lung cancer by suppressing tumor cell invasiveness. *Cancer Res* 2006;**66**:11763–70
45. Scopetti D, Piobbico D, Brunacci C, Pieroni S, Bellezza G, Castelli M, Ludovini V, Tofanetti FR, Cagini L, Sidoni A, Puxeddu E, Della-Fazia MA, Servillo G. INSL4 as prognostic marker for proliferation and invasiveness in non-small-cell lung cancer. *J Cancer* 2021;**12**:3781–95
46. Yang R, Li SW, Chen Z, Zhou X, Ni W, Fu DA, Lu J, Kaye FJ, Wu L. Role of INSL4 signaling in sustaining the growth and viability of LKB1-inactivated lung cancer. *J Natl Cancer Inst* 2019;**111**:664–74
47. Hellmann MD, Paz-Ares L, Bernabe Caro R, Zurawski B, Kim SW, Carcereny Costa E, Park K, Alexandru A, Lupinacci L, de la Mora Jimenez E, Sakai H, Albert I, Vergnenegre A, Peters S, Syrigos K, Barlesi F, Reck M, Borghaei H, Brahmer JR, O'Byrne KJ, Geese WJ, Bhagavatheeswaran P, Rabindran SK, Kasinathan RS, Nathan FE, Ramalingam SS. Nivolumab plus ipilimumab in advanced non-small-cell lung cancer. *N Engl J Med* 2019;**381**:2020–31
48. Paz-Ares L, Luft A, Vicente D, Tafreshi A, Gümüş M, Mazières J, Hermes B, Çay Şenler F, Csőszi T, Fülöp A, Rodríguez-Cid J, Wilson J, Sugawara S, Kato T, Lee KH, Cheng Y, Novello S, Halmos B, Li X, Lubiniecki GM, Piperdi B, Kowalski DM. Pembrolizumab plus chemotherapy for squamous non-small-cell lung cancer. *N Engl J Med* 2018;**379**:2040–51
49. Chen DS, Mellman I. Elements of cancer immunity and the cancer-immune set point. *Nature* 2017;**541**:321–30
50. Morad G, Helmink BA, Sharma P, Wargo JA. Hallmarks of response, resistance, and toxicity to immune checkpoint blockade. *Cell* 2021; **184**:5309–37


*(Received February 2, 2022, Accepted April 23, 2022)*